TRUE COVARIANCE SIMULATION OF THE EUVE UPDATE FILTER

by

I. Y. Bar-Itzhack* and R. R. Harman**
NASA - Goddard Space Flight Center
Greenbelt MD, 20771

Abstract

This paper presents a covariance analysis of the performance and sensitivity of the attitude determination Extended Kalman Filter (EKF) used by the On Board Computer (OBC) of the Extreme Ultra Violet Explorer (EUVE) spacecraft. The linearized dynamics and measurement equations of the error states are derived which constitute the "truth model" describing the real behavior of the systems involved. The "design model" used by the OBC EKF is then obtained by reducing the order of the truth model. The covariance matrix of the EKF which uses the reduced order model is not the correct covariance of the EKF estimation error. A "true covariance analysis" has to be carried out in order to evaluate the correct accuracy of the OBC generated estimates. The results of such analysis are presented which indicate both the performance and the sensitivity of the OBC EKF.

1.0 INTRODUCTION

The Extreme Ultraviolet Explorer (EUVE) is scheduled to be launched by a Delta launch vehicle in August 1990 into a 550 km orbit with a 28.5 degree inclination. The EUVE experiment will observe stellar objects emitting electromagnetic radiation with wavelengths of 100 to 1000 angstroms. The spacecraft design is called an Explorer Platform (EP). The EP is designed to be flexible enough to be used by many different experiments. The EP consists of three main modules: experiment, Platform Equipment Deck (PED), and the multimission modular spacecraft (MMS). The MMS contains the attitude control system, power system, and the command and data handling system. The EUVE mission is divided into two phases: all sky survey and spectroscopy. In the all sky survey, the spacecraft will be rotating at 3 revolutions per orbit (3 RPO about the roll axis) while instruments perpendicular to the roll axis scan the sky. Six months later, EUVE will be three axis stabilized at selected spectroscopic targets.

2.0 ALGORITHM

2.1 INTRODUCTION

The attitude of the Explorer Platform (EP) is determined by gyros which measure the angular rate vector of the EP, by two fixed-head star trackers (FHST), and by one fine sun sensor (FSS). The gyros yield three components of the angular rate vector of the EP rotation with respect to inertial space. The components measured by the gyros are the projections of the vector on the body axes, which are the axes of the attitude control system (ACS).

If the exact orientation of the ACS with respect to inertial coordinates is known at some point, if the gyro outputs are perfect, and if no computation errors are introduced when solving the attitude propagation equations, then from that time on the EP attitude is known exactly. However, since the initial knowledge of the attitude is never perfect, since the gyro outputs include measurement and misalignment errors, and since the computation is not perfect either, the attitude of the EP is not perfectly known. Moreover, the attitude errors tend to diverge and consequently corrections of the computed attitude have to be performed. This is the reason for employing two FHSTs and one FSS in attitude determination.

Star tracker and Sun sensor measurements, when used correctly, check the attitude error growth. The information supplied by the FHSTs and by the FSS is blended with the attitude computed based on the gyro outputs and on the initial EP orientation. This blending is done by a Kalman filter (KF). The EP on board computer (OBC) software uses quaternions for attitude determination. The relationship between vector measurements, which are the outputs of the FHSTs and of the FSS, and the quaternion of rotation is non-linear. Therefore an Extended Kalman filter (EKF), rather than a KF, has to be employed.

For simplicity of implementation the EKF used by the OBC is actually a reduced order suboptimal filter which does not contain all the error sources in the gyros, in the FHSTs and in the FSS [1,2]. It is, therefore, necessary to investigate the predicted performance of the on board reduced order EKF. To evaluate the performance of the EKF, finer error models have to be used in describing the performance of the true hardware [3,4]. Such models are referred to in the literature as "truth models" [5]. In this paper we introduce a "truth model" which takes in account factors neglected in the OBC EKF model. These factors are gyro, FHST and FSS misalignments, gyro scale factor errors and the effect of the Sun not being captured in a narrow field of view about the boresight of the FSS.

A convenient analysis tool is the "true covariance" simulation [6]. This paper presents such analysis of the performance of the on board attitude determination EKF of the EUVE satellite. The "truth model" of the attitude determination problem is developed next. The "design model" is then listed in Section 2.3. Next the "true covariance" simulation algorithm is presented in Section 3. The analysis which was carried out and its results are presented in Section 4 and finally, the conclusions drawn from this analysis are presented in Section 5.

2.2 THE TRUTH MODEL

Error Propagation Model

Open-loop attitude determination

Consider Fig. 1 which describes a generic attitude control spacecraft (S/C). The input quaternion, q_i, represents a command attitude and q_t is the quaternion which represents the actual attitude of the S/C. As shown in Fig. 1, gyros which are mounted on the S/C

---

*NRC NASA Resident Research Associate. On Sabbatical leave from the Aerospace Engineering Dept., Technion - Israel Institute of Tecnology, Haifa 32000, Israel.

**Aerospace Engineer, Attitude Analysis Section, Flight Dynamics Analysis Branch.

measure its angular velocity. The readings of these gyros are used by the Attitude Determination algorithm to compute the quaternion q_c which represents the computed attitude. This configuration is called "open-loop" since here q_c is not fed back

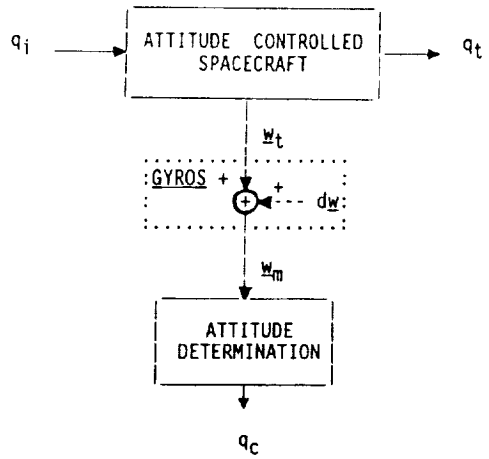

Fig. 1: Generic open-loop attitude determination configuration

into the attitude controlled S/C. Consequently in this configuration the gyro error, $d\underline{w}$, of these gyros is not affecting the S/C attitude.

Let us denote by "i" the inertial coordinate system which is the reference coordinate system and by "a" the ACS coordinate system which which we assume to be identical to the body system. The attitude determination problem is that of finding the quaternion which corresponds to the transformation matrix from "i" to "a" (or vice-versa). Since the gyros introduce measurement errors ($d\underline{w}$) the computed attitude is erroneous. Therefore the computed transformation matrix which is supposed to transform vectors from the "i" to the "a" frame, actually transforms the vectors from the "i" frame to another erroneous coordinate system which we denote by "c". Thus we distinguish between three coordinate systems; namely, the "i", the "a" and the "c" systems. We assume that the error in computing the transformation matrix is small, consequently "a" and "c" are almost identical. In other words, a very small transformation takes us from

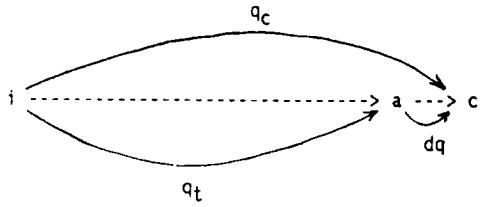

Fig. 2: Schematic description of the quaternion relations in the attitude determination problem

the "a" to the "c" system. To the transformations between the coordinates there correspond suitable quaternions as depicted in Fig. 2. As indicated in this diagram

$$q_t = q_{i\text{-to-}a} \tag{1.a}$$

$$q_c = q_{i\text{-to-}c} \tag{1.b}$$

$$dq = q_{a\text{-to-}c} \tag{1.c}$$

The subscript "t" corresponds to the transformation to the true attitude of the vehicle whereas the subscript "c" denotes the transformation to the computed attitude. (Note that "c" corresponds to the subscripted notation 'measured' in refs. 2 and 3). When defining a quaternion of rotation and especially when dealing with quaternion products, a special care has to be given to the question of what coordinate frame the quaternion is referred to. If each of the three quaternions defined is referred to the coordinate system from which it transforms vectors, then the following relation between them holds

$$q^i_{i\text{-to-}c} = q^i_{i\text{-to-}a}\, q^a_{a\text{-to-}c} \tag{2}$$

where the product on the right hand side of (2) is the quaternion product (defined in the Appendix) and the superscripts denote the frame to which each quaternion is referred*. From (1.c) the rightmost quaternion in (2) is dq. Note that dq is the only quaternion referred to the body frame whereas the other two are referred to the inertial frame. Keeping this in mind we omit all superscripts and use the notations of (1) to write (2) as

$$\boxed{q_c = q_t dq} \tag{3}$$

Differentiation of (3) yields

$$\dot{q}_c = \dot{q}_t dq + q_t d\dot{q} \tag{4}$$

It is well known [7] that

$$\dot{q}_t = \frac{1}{2} q_t W \tag{5}$$

where W is a quaternion of angular velocities defined as follows

$$W = iw_x + jw_y + kw_z \tag{6}$$

The components w_x, w_y, w_z are the components of the true angular velocity vector at which the ACS coordinate frame rotates with respect to the inertial frame, coordinatized in the ACS frame. These components are measured by gyros which supply measured (and hence erroneous) data. In the lack of knowledge of the true rates, the gyro outputs are used in computing the quaternion, therefore the solution of (5) yields q_c rather than q_t; that is, q_c is the solution of

$$\dot{q}_c = \frac{1}{2} q_c W_m \tag{7}$$

* Note that $q^i_{i\text{-to-}c} = q^i_{a\text{-to-}c}\, q^i_{i\text{-to-}a}$; that is, when all quaternions are referred to the inertial frame the order of the product is reversed.

where W_m is of the form of (6) only that the quaternion components are the measured rather than the exact angular rates.

When (5) and (7) are substituted into (4) we obtain

$$\frac{1}{2}q_c W_m = \frac{1}{2}q_t W\, dq + q_t d\dot{q} \qquad (8)$$

Define a quaternion of angular-rate error as follows

$$dW = W_m - W$$

then

$$W = W_m - dW \qquad (9)$$

Substituting (9) and (3) into (8) yields

$$\frac{1}{2}q_t dq W_m = \frac{1}{2}q_t(W_m - dW)dq + q_t d\dot{q}$$

which can be written as

$$q_t\left[d\dot{q} + \frac{1}{2}(W_m - dW)dq - \frac{1}{2}dqW_m\right] = 0$$

Since q_t is invertible, it is possible to pre-multiply both sides of the last equation by the inverse of q_t. This yields the result that the expression in the brackets is equal to zero and consequently

$$\boxed{d\dot{q} = \frac{1}{2}dqW_m - \frac{1}{2}W_m dq + \frac{1}{2}dWdq} \qquad (10)$$

Let us express the quaternions appearing in (10) in a more explicit form by their vector and scalar parts. Accordingly

$$dq = \begin{bmatrix} d\underline{\phi} \\ \cdots \\ d\theta \end{bmatrix} \qquad W_m = \begin{bmatrix} \underline{w}_m \\ \cdots \\ 0 \end{bmatrix}$$

where $d\underline{\phi}$ is the vector part of the quaternion. When the quaternion product is carried out (see the Appendix for the rules of quaternion product), (10) reads as follows

$$\begin{bmatrix} d\dot{\underline{\phi}} \\ \cdots \\ d\dot{\theta} \end{bmatrix} = \frac{1}{2}\begin{bmatrix} d\underline{\phi}\times\underline{w}_m + d\theta\underline{w}_m \\ \cdots \\ -d\underline{\phi}.\underline{w} \end{bmatrix} - \frac{1}{2}\begin{bmatrix} \underline{w}_m\times d\underline{\phi} + d\theta\underline{w}_m \\ \cdots \\ -\underline{w}.d\underline{\phi} \end{bmatrix}$$

$$+ \frac{1}{2}\begin{bmatrix} d\underline{w}\times d\underline{\phi} + d\theta d\underline{w} \\ \cdots \\ -d\underline{w}.d\underline{\phi} \end{bmatrix}$$

The last quaternion equation is equivalent to two equations, one for the vector part of q and one for its scalar part. Using the following rules of vector product, $\underline{A}\times\underline{B} = -\underline{B}\times\underline{A}$ and $\underline{A}.\underline{B} = \underline{B}.\underline{A}$, the two equations can be written as

$$d\dot{\underline{\phi}} = -\underline{w}_m\times d\underline{\phi} + \frac{1}{2}d\theta d\underline{w} + \frac{1}{2}d\underline{w}\times d\underline{\phi} \qquad (11.a)$$

$$d\dot{\theta} = -d\underline{w}.d\underline{\phi} \qquad (11.b)$$

When dq expresses a small rotation, its vector part, $d\underline{\phi}$, is small, therefore the last term on the right hand side of (11.a) is of second order and hence is negligible. The right hand side of (11.b) is negligible too and indeed, since the absolute value of any quaternion of rotation is equal to 1, the scalar part of dq satisfies the equation $d\theta = [1 - |d\underline{\phi}|^2]^{1/2}$ and since the vector part is small, $d\theta$, stays close to 1, hence its time derivative is nearly zero. Note that as $d\theta$ is nearly 1, the second term on the right hand side of (11.a) is not negligible. Consequently (11) yields

$$d\dot{\underline{\phi}} \sim -\underline{w}_m\times d\underline{\phi} + \frac{1}{2}d\underline{w} \qquad (12.a)$$

and as explained above

$$d\theta \sim 1 \qquad (12.b)$$

The equation of interest is (12.a).

The transformation matrix T_c^a which corresponds to dq can be expressed in terms of small Euler angles. Define the angles as follows

φ is the roll angle error defined about the body x-axis
ϑ is the pitch angle error defined about the body y-axis
ψ is the yaw angle error defined about the body z-axis.

Note that for small rotations the order of rotation is irrelevant and we may refer all angles to the initial coordinate system which prevailed before the small rotations took place. Also note that these angles are referred to the body frame, "a", as is implied in (2) and (3). When the transformation matrix from the body to the computed frame is expressed as a function of the three Euler angles defined above and when the angles approach zero, the transformation matrix becomes

$$T_c^a = \begin{bmatrix} 1 & \psi & -\vartheta \\ -\psi & 1 & \varphi \\ \vartheta & -\varphi & 1 \end{bmatrix} \qquad (13)$$

On the other hand, in terms of the components of dq, the upper right elements of T_c^a are [8]

$$t_{1,2} = 2dq_1dq_2 + 2dq_3dq_4 \qquad (14.a)$$

$$t_{1,3} = 2dq_1dq_3 - 2dq_2dq_4 \qquad (14.b)$$

$$t_{2,3} = 2dq_2dq_3 + 2dq_1dq_4 \qquad (14.c)$$

The first term on the right hand side of each one of the above equations is of second order and hence is negligible. On the other hand, dq_4 appearing in the second term is the scalar part of dq which we denoted by $d\theta$. As noted earlier this component is nearly equal to one. For these reasons (14) can be approximated as follows

$$t_{1,2} \sim 2dq_3 \qquad (15.a)$$

$$t_{1,3} \sim -2dq_2 \qquad (15.b)$$

$$t_{2,3} \sim 2dq_1 \qquad (15.c)$$

Comparing (15) to the corresponding elements in (13) yields

$$dq_1 = \frac{1}{2}\varphi$$

$$dq_2 = \frac{1}{2}\vartheta$$

$$dq_3 = \frac{1}{2}\psi$$

The above three components of q constitute the elements of $\underline{\Phi}$, thus

$$d\underline{\Phi} = \frac{1}{2}\begin{vmatrix} \varphi \\ \vartheta \\ \psi \end{vmatrix} \qquad (16)$$

and (12.a) can be written as

$$\begin{vmatrix} \dot{\varphi} \\ \dot{\vartheta} \\ \dot{\psi} \end{vmatrix} = \begin{vmatrix} 0 & w_z & -w_y \\ -w_z & 0 & w_x \\ w_y & -w_x & 0 \end{vmatrix} \begin{vmatrix} \varphi \\ \vartheta \\ \psi \end{vmatrix} + \begin{vmatrix} dw_x \\ dw_y \\ dw_z \end{vmatrix} \qquad (17)$$

Closed-loop attitude determination

In the case of a closed-loop attitude determination, the S/C is maintained at a desired (possibly time-varying) attitude by a closed control loop which uses the gyro outputs to keep track of the S/C angular rate. This is shown in Fig. 3 in which a part of the control loop of a generic attitude control system of a S/C is presented. The purpose of this control loop is to force the S/C to follow a prescribed angular velocity vector, $\underline{w}_i$, and in particular to maintain a constant attitude when $\underline{w}_i=0$. (Normally the commanded rate $\underline{w}_i$ is a function of the difference between a commanded quaternion and the computed quaternion, q_c). We note from Fig. 3 that

$$\bar{\underline{w}} = \underline{w}_i - \underline{w}_c \qquad (18)$$

The control loop is designed to force $\bar{\underline{w}}$ to vanish, then

$$\underline{w}_c = \underline{w}_i \qquad (19)$$

and since

$$\underline{w}_c = \underline{w} + d\underline{w} \qquad (20)$$

therefore

$$\underline{w}_i = \underline{w} + d\underline{w}$$

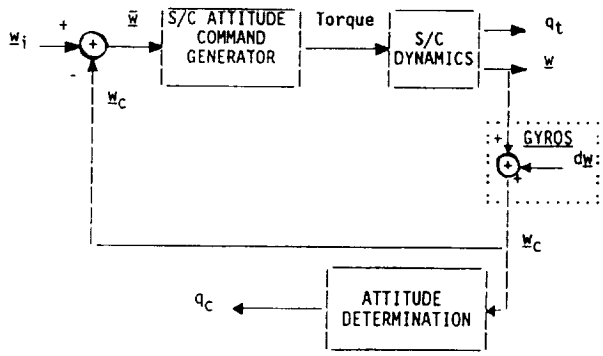

Fig. 3: Generic rate command control loop part of a spacecraft attitude control system

Consequently, $\underline{w}$, the actual angular rate of the S/C differs from the desired angular rate vector, $\underline{w}_i$, by the gyro drift rate vector, $d\underline{w}$; that is

$$\underline{w} = \underline{w}_i - d\underline{w} \qquad (21)$$

and in particular when $\underline{w}_i = 0$; that is, when the S/C is required to maintain a constant attitude

$$\underline{w} = -d\underline{w} \qquad (22)$$

that is; the S/C drifts at the drift rate of the gyros but in a direction opposite to the gyro drift. We conclude from this discussion that $\underline{w}$ differs from the commanded rate by $d\underline{w}$. Consequently the attitude of the S/C differs from the commanded attitude by the attitude error angles φ, ϑ, and ψ. In this case therefore, the attitude errors develop according to the following equation rather than according to (17)

$$\begin{vmatrix} \dot{\varphi} \\ \dot{\vartheta} \\ \dot{\psi} \end{vmatrix} = \begin{vmatrix} 0 & w_z & -w_y \\ -w_z & 0 & w_x \\ w_y & -w_x & 0 \end{vmatrix} \begin{vmatrix} \varphi \\ \vartheta \\ \psi \end{vmatrix} - \begin{vmatrix} dw_x \\ dw_y \\ dw_z \end{vmatrix} \qquad (23)$$

Indeed when the commanded angular rate is zero (23) yields

$$\dot{\varphi} = -dw_x, \quad \dot{\vartheta} = -dw_y \text{ and } \dot{\psi} = -dw_z$$

The right most term in (23) is not a white noise vector, therefore this dynamic model, while correct, is not suitable for use in a KF algorithm. To solve this difficulty the standard procedure of "signal shaping" is applied. This is done by considering the non-white vector as an output of a linear system whose input is white [5]. This is accomplished as follows.

The elements dw_x, dw_y, dw_z are the errors in measuring $\underline{w}$. In other words, they are the errors in the x,y and z gyros respectively. It is assumed that an accurate enough model of the gyro errors is a one where there are five contributions to $d\underline{w}$, which we denote by $\underline{u}_1$, $\underline{u}_2$, $d\underline{s}$, $\underline{w}_\phi$ and $\underline{n}_1$; that is,

$$d\underline{w} = \underline{u}_1 + \underline{u}_2 + d\underline{s} + \underline{w}_\phi + \underline{n}_1 \qquad (24.a)$$

where $\underline{u}_1$ is a vector of constant drift rates of the gyros, $\underline{u}_2$ is a vector of random walk components of the gyros, $d\underline{s}$ is the vector of gyro scale factor errors and

$\underline{w}_\phi$ is the error due to gyro misalignments. $\underline{n}_1$ is the white noise component of the gyros. Since $\underline{u}_1$ is constant

$$\dot{\underline{u}}_1 = 0 \qquad (24.b)$$

and since $\underline{u}_2$ is random walk then we can write

$$\dot{\underline{u}}_2 = \underline{n}_2 \qquad (24.c)$$

where $\underline{n}_2$ is white noise. Note that despite the notation, $\underline{n}_2$ does not have the units of angular velocity. Let us denote the vector of scale factor errors by $\underline{k}$, then

$$\underline{k}' = [k_x, k_y, k_z] \qquad (24.d)$$

where ' denotes the transpose and k_x, k_y and k_z are the scale factor errors of the x, y and z gyros respectively. The expression for $d\underline{s}$ is given by

$$d\underline{s} = \begin{bmatrix} w_x & 0 & 0 \\ 0 & w_y & 0 \\ 0 & 0 & w_z \end{bmatrix} \underline{k} \qquad (24.e)$$

Note that since $\underline{k}$ is a constant

$$\dot{\underline{k}} = 0 \qquad (24.f)$$

The gyro errors due to misalignments are generated by the projection on the gyro input axis of the angular velocity components which are nominally perpendicular to that axis. The misalignment angles are the angles by which the gyro sensitive axis is off from its nominal orthogonal direction towards the other two coordinate axes. Consequently we have

$$\underline{w}_\phi = \begin{bmatrix} w_{\phi x} \\ w_{\phi y} \\ w_{\phi z} \end{bmatrix} = \begin{bmatrix} w_y & w_z & 0 & 0 & 0 & 0 \\ 0 & 0 & w_z & w_x & 0 & 0 \\ 0 & 0 & 0 & 0 & w_x & w_y \end{bmatrix} \begin{bmatrix} \phi_{xy} \\ \phi_{xz} \\ \phi_{yz} \\ \phi_{yx} \\ \phi_{zx} \\ \phi_{zy} \end{bmatrix} \qquad (24.g)$$

where ϕ_{ij} i=a,y,z j=x,y,z is the non-orthogonality angle between the i-th gyro and the j-th axis. Now since ϕ_{ij} is constant we can write

$$\dot{\phi}_{ij} = 0 \qquad \begin{matrix} i=x,y,z \\ j=x,y,z \end{matrix} \qquad (24.h)$$

The next step in the derivation of the dynamics matrix is the augmentation of the system error model given in (23) with the gyro error model given in (24) [5]. Such an augmented model has, in our case, 27 states. Fortunately, we can eliminate 3 states by combining the constant drift rate components and the random walk components into one error. This will eliminate the possibility of distinguishing between them, but this is of no great consequence since even if we can estimate them separately, we subtract them both from the reading of the gyro outputs in order to obtain more accurate gyro measurements, therefore the same result is achieved when we estimate their sum. When we combine $\underline{u}_1$ and $\underline{u}_2$ into one state denoted by $\underline{u}$, we may use (24.b) and (24.c) to write the dynamic model of $\underline{u}$

$$\dot{\underline{u}} = \underline{n}_2 \qquad (24.i)$$

In order to augment the models presented in (23) and (24) we define the following matrices

$$\underline{x}^* = \begin{bmatrix} \varphi \\ \upsilon \\ \psi \\ u_x \\ u_y \\ u_z \end{bmatrix} \qquad A^* = \begin{bmatrix} 0 & w_z & -w_y & -1 & 0 & 0 \\ -w_z & 0 & w_x & 0 & -1 & 0 \\ w_y & -w_x & 0 & 0 & 0 & -1 \\ 0 & 0 & 0 & 0 & 0 & 0 \\ 0 & 0 & 0 & 0 & 0 & 0 \\ 0 & 0 & 0 & 0 & 0 & 0 \end{bmatrix} \qquad \ldots\ldots (25)$$

$$-\underline{n}^* = \begin{bmatrix} n_{1x} \\ n_{1y} \\ n_{1z} \\ n_{2x} \\ n_{2y} \\ n_{2z} \end{bmatrix} \qquad A^{**} = \begin{bmatrix} -w_x & 0 & 0 & -w_y & -w_z & 0 & 0 & 0 & 0 \\ 0 & -w_y & 0 & 0 & 0 & -w_z & -w_x & 0 & 0 \\ 0 & 0 & -w_z & 0 & 0 & 0 & 0 & -w_x & -w_y \\ 0 & 0 & 0 & 0 & 0 & 0 & 0 & 0 & 0 \\ 0 & 0 & 0 & 0 & 0 & 0 & 0 & 0 & 0 \\ 0 & 0 & 0 & 0 & 0 & 0 & 0 & 0 & 0 \end{bmatrix} \qquad \ldots (26)$$

$$\underline{\phi}' = [\phi_{xy}, \phi_{xz}, \phi_{yz}, \phi_{yx}, \phi_{zx}, \phi_{zy}] \qquad (27)$$

We may also want to consider the misalignment angles of the two FHSTs and of the FSS, therefore let us denote the vector of the three misalignment angles of the first FHST by ${}^1\underline{\phi}$, that of the second FHST by ${}^2\underline{\phi}$ and the vector of the FSS misalignment angles by ${}^s\underline{\phi}$ where

$${}^1\underline{\phi}' = [{}^1\phi_x, {}^1\phi_y, {}^1\phi_z] \qquad (28.a)$$

$${}^2\underline{\phi}' = [{}^2\phi_x, {}^2\phi_y, {}^2\phi_z] \qquad (28.b)$$

$${}^s\underline{\phi}' = [{}^s\phi_x, {}^s\phi_y, {}^s\phi_z] \qquad (28.c)$$

Since all of these angles are constants we may write

$${}^1\dot{\underline{\phi}} = 0 \qquad {}^2\dot{\underline{\phi}} = 0 \qquad {}^s\dot{\underline{\phi}} = 0 \qquad (29)$$

With the above information and notations we can now write the augmented dynamics equation of the "truth model". The augmented dynamics equation of the "truth model" is given in (30). The validity of (30) can be verified by examining (23) - (29).

$$\frac{d}{dt}\begin{bmatrix} \underline{X}^* \\ \underline{k} \\ \underline{\phi} \\ {}^1\underline{\phi} \\ {}^2\underline{\phi} \\ {}^s\underline{\phi} \end{bmatrix} = \begin{bmatrix} A^* & A^{**} & 0 & 0 & 0 \\ 0 & 0 & 0 & 0 & 0 \\ 0 & 0 & 0 & 0 & 0 \\ 0 & 0 & 0 & 0 & 0 \\ 0 & 0 & 0 & 0 & 0 \\ 0 & 0 & 0 & 0 & 0 \end{bmatrix} \begin{bmatrix} \underline{X}^* \\ \underline{k} \\ \underline{\phi} \\ {}^1\underline{\phi} \\ {}^2\underline{\phi} \\ {}^s\underline{\phi} \end{bmatrix} + \begin{bmatrix} \underline{n}^* \\ \underline{0} \\ \underline{0} \\ \underline{0} \\ \underline{0} \\ \underline{0} \end{bmatrix} \quad \ldots (30)$$

Measurement Model

Star tracker measurements

Define a star tracker coordinate system as shown in Fig. 4. The z axis points along the boresight of the star tracker. Consequently the x and y axes are in the image-plane of the star tracker. Denote by $\underline{S}^*$ the vector in the direction of the star and whose length is the length of the light path from the image-plane to the optics. It is assumed that the light which is emitted from the star towards which the star tracker is pointing, hits the image-plane close to the boresight such that it can be assumed that the distance between the optics and the image plane is nearly equal to that of the light path from the optics to the image-plane, i.e. $h-|\underline{S}|$. The signals measured by the tracker are the projections of $-\underline{S}$ on the x and the y axes which, as mentioned, are in the image-plane. The OBC converts the two outputs of the star tracker to tangents of A and B. Obviously, the tangents of A and of B are, respectively, the projections of $-\underline{S}$ on the x and y axes of the tracker, where $\underline{S}$ is a unit vector in the direction of the star. That is, if we denote these axes by $\underline{x}_{st}$ and $\underline{y}_{st}$ respectively, then

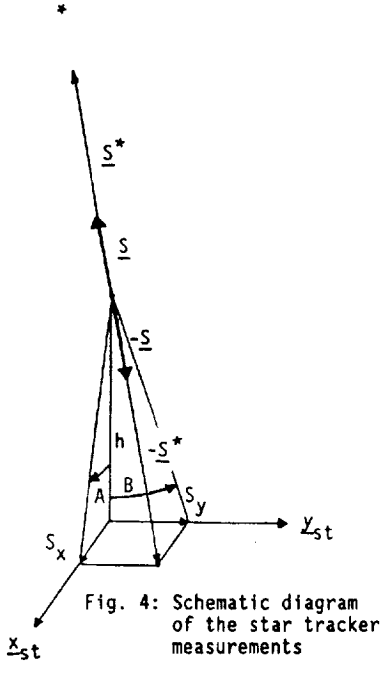

Fig. 4: Schematic diagram of the star tracker measurements

$$x_m = -\underline{S}\cdot\underline{x}_{st} + e_x \quad \ldots (31.a)$$

$$y_m = -\underline{S}\cdot\underline{y}_{st} + e_y \quad \ldots (31.b)$$

where x_m and y_m are the tangents of A and B, "$\cdot$" denotes the dot product of vectors and e_x and e_y are measurement noise signals which are assumed to be zero-mean white processes. (Actually, the OBC converts x_m and y_m into components of the unit vector $\underline{S}$. For small A and B these components are basically equal to the respective tangents). Let us now express the vector quantities of (31) in the EP body coordinate system

$$x_m = -\underline{S}_a\cdot(\underline{x}_{st})_a + e_x \quad (32.a)$$

$$y_m = -\underline{S}_a\cdot(\underline{y}_{st})_a + e_y \quad (32.b)$$

We use an under-bar and a subscript to denote a column matrix whose elements are the components of the vector in question when resolved in the coordinate system denoted by the subscript.

The observables (also known as effective measurements) which are processed by the EKF are the difference between measured and computed quantities. For star tracker measurements we feed the EKF with the difference between the measured components x and y given in (32) and the corresponding computed values which are obtained by transforming the star vector from inertial to body coordinates. The star vector coordinatized in the inertial frame, which we denote by $\underline{S}_I$, is precisely known from the almanac. We do not know, however, the exact value of T_a^I, the transformation matrix from inertial to body system. All we know is the computed transformation matrix T_c^I. The relationship between the two matrices is given by

$$T_c^I = T_c^a T_a^I \quad (33)$$

where T_a^b is the error matrix given in (13). If we define the matrix θ as follows

$$\theta = \begin{bmatrix} 0 & \psi & -\vartheta \\ -\psi & 0 & \varphi \\ \vartheta & -\varphi & 0 \end{bmatrix} \quad (34)$$

then

$$T_c^a = I + \theta \quad (35)$$

We also do not know the exact direction of $\underline{x}_{st}$ and $\underline{y}_{st}$ since the star tracker is misaligned. We only know $\underline{x}_{st,ass.}$ and $\underline{y}_{st,ass.}$ which are the vectors $\underline{x}_{st}$ and $\underline{y}_{st}$ in the ***assumed*** coordinate system of the FHST (that is, in the non misaligned FHST). Consequently, the computed values are calculated in correspondence with (32) as follows

$$x_c = -(T_c^I\underline{S}_I)\cdot(\underline{x}_{st,ass})_a \quad (36.a)$$

$$y_c = -(T_c^I\underline{S}_I)\cdot(\underline{y}_{st,ass})_a \quad (36.b)$$

Using (33) and (35) these two equations become

$$x_c = -[(I+\theta)T_a^I\underline{S}_I]\cdot(\underline{x}_{st,ass})_a \quad (37.a)$$

$$y_c = -[(I+\theta)T_a^I\underline{S}_I]\cdot(\underline{y}_{st,ass})_a \quad (37.b)$$

We note that

$$T_a^I\underline{S}_I = \underline{S}_a \quad (38)$$

therefore (37) can be written as

$$x_c = -[\underline{S}_a + \theta\underline{S}_a]\cdot(\underline{x}_{st,ass})_a \quad (39.a)$$

$$y_c = -[\underline{S}_a + \theta\underline{S}_a]\cdot(\underline{y}_{st,ass})_a \quad (39.b)$$

When we now difference (32) and (39) the following equations are obtained

$$z_1 = x_m - x_c = -\underline{S}_a\cdot(\underline{x}_{st})_a + e_x + [\underline{S}_a + \theta\underline{S}_a]\cdot(\underline{x}_{st,ass})_a \quad \ldots (40.a)$$

$$z_2 = y_m - y_c = -\underline{S}_a\cdot(\underline{y}_{st})_a + e_y + [\underline{S}_a + \theta\underline{S}_a]\cdot(\underline{y}_{st,ass})_a \quad \ldots (40.b)$$

We note that

$$\underline{x}_{st} = M_T^{T,ass}\, \underline{x}_{st,ass} \qquad (41.a)$$

$$\underline{y}_{st} = M_T^{T,ass}\, \underline{x}_{st,ass} \qquad (41.b)$$

where $M_T^{T,ass}$ is the transformation matrix from the assumed FHST coordinate system to the actual one. In analogy to (35) it can also be shown that

$$M_T^{T,ass} = I - [\underline{\phi}x] \qquad (42)$$

where

$$-[\underline{\phi}x] = \begin{vmatrix} 0 & \phi_z & -\phi_y \\ -\phi_z & 0 & \phi_x \\ \phi_y & -\phi_x & 0 \end{vmatrix} \qquad (43)$$

The angles ϕ_i $i=x,y,z$ are the misalignment angles of the actual FHST coordinates with respect to the assumed FHST coordinates. Note that because of the closeness of the two, the angles are the same in either coordinates. (See development leading to (56)). When we substitute (42) into (41) we obtain

$$\underline{x}_{st} = (I - [\underline{\phi}x])\, \underline{x}_{st,ass} \qquad (44.a)$$

$$\underline{y}_{st} = (I - [\underline{\phi}x])\, \underline{y}_{st,ass} \qquad (44.b)$$

hence

$$\underline{x}_{st} = \underline{x}_{st,ass} - \underline{\phi} \times \underline{x}_{st,ass} \qquad (45.a)$$

$$\underline{y}_{st} = \underline{y}_{st,ass} - \underline{\phi} \times \underline{y}_{st,ass} \qquad (45.b)$$

When (45) are substituted into (40) the following is obtained

$$z_1 = -\underline{S}_a \cdot (\underline{x}_{st,ass} - \underline{\phi} \times \underline{x}_{st,ass})_a + e_x + [\underline{S}_a + \Theta \underline{S}_a] \cdot (\underline{x}_{st,ass})_a$$

$$z_2 = -\underline{S}_a \cdot (\underline{y}_{st,ass} - \underline{\phi} \times \underline{y}_{st,ass})_a + e_y + [\underline{S}_a + \Theta \underline{S}_a] \cdot (\underline{y}_{st,ass})_a$$

which, after some multiplications and subtractions, yields

$$z_1 = \underline{S}_a \cdot (\underline{\phi} \times \underline{x}_{st,ass})_a + \Theta \underline{S}_a \cdot (\underline{x}_{st,ass})_a + e_x \qquad (46.a)$$

$$z_2 = \underline{S}_a \cdot (\underline{\phi} \times \underline{y}_{st,ass})_a + \Theta \underline{S}_a \cdot (\underline{y}_{st,ass})_a + e_y \qquad (46.b)$$

For (46) to be useful, we need to evaluate $\underline{S}_a$, $(\underline{x}_{st,ass})_a$ and $(\underline{y}_{st,ass})_a$. As mentioned earlier, $\underline{S}_I$ is known from the almanac, therefore

$$\underline{S}_a = T_a^I\, \underline{S}_I \qquad (47)$$

We do not know T_a^I but we do know T_c^I which, for small attitude errors, is quite close to T_a^I. The replacement of the true value by its estimate is one of the features of an EKF, so, we too, follow this practice, compute

$$\underline{S}_c = T_c^I\, \underline{S}_I \qquad (48)$$

and use $\underline{S}_c$ rather than $\underline{S}_a$ in (46). Next we handle the computation of $(\underline{x}_{st,ass})_a$ and $(\underline{y}_{st,ass})_a$. It is clear that

$$(\underline{x}_{st,ass})_a = M_a^{T,ass} (\underline{x}_{st,ass})_{T,ass} \qquad (49.a)$$

$$(\underline{y}_{st,ass})_a = M_a^{T,ass} (\underline{y}_{st,ass})_{T,ass} \qquad (49.b)$$

where T denotes the star tracker coordinate system defined at the beginning of this section and $M_a^{T,ass}$ is the transformation matrix from the assumrd tracker frame to the body frame. This matrix is known precisely. Let us write

$$M_a^{T,ass} = [\ \underline{m}_1,\ \underline{m}_2,\ \underline{m}_3\ ] \qquad (50)$$

where $\underline{m}_1$, $\underline{m}_2$ and $\underline{m}_3$ are the three columns of $M_a^{T,ass}$. It is clear that $(\underline{x}_{st,ass})_T$, the unit vector along the tracker assumed x axis expressed in tracker coordinates, is given by

$$(\underline{x}_{st,ass})_T = \begin{vmatrix} 1 \\ 0 \\ 0 \end{vmatrix} \qquad (51.a)$$

and similarly

$$(\underline{y}_{st,ass})_T = \begin{vmatrix} 0 \\ 1 \\ 0 \end{vmatrix} \qquad (51.b)$$

Therefore when (50) and (51) are substituted into (49), the following is obtained

$$(\underline{x}_{st,ass})_a = \underline{m}_1 \qquad (52.a)$$

$$(\underline{y}_{st,ass})_a = \underline{m}_2 \qquad (52.b)$$

When (52) is substituted into (46), and when $\underline{S}_a$ is replaced in (46) by $\underline{S}_c$ which is given in (48), the following is obtained

$$z_1 = \underline{S}_c \cdot [(\underline{\phi})_a \times \underline{m}_1] + \Theta \underline{S}_c \cdot \underline{m}_1 + e_x \qquad (53.a)$$

$$z_2 = \underline{S}_c \cdot [(\underline{\phi})_a \times \underline{m}_2] + \Theta \underline{S}_c \cdot \underline{m}_2 + e_y \qquad (53.b)$$

Noting that

$$\Theta = -[\underline{\theta}_a x]$$

and using the vector identity

$$(\bar{A} \times \bar{B}) \cdot \bar{C} = (\bar{B} \times \bar{C}) \cdot \bar{A}$$

equations (53) can be written as

$$z_1 = (\underline{m}_1 \times \underline{S}_c) \cdot \underline{\phi}_a + (\underline{m}_1 \times \underline{S}_c) \cdot \underline{\theta}_a + e_x \qquad (54.a)$$

$$z_2 = (\underline{m}_2 \times \underline{S}_c) \cdot \underline{\phi}_a + (\underline{m}_2 \times \underline{S}_c) \cdot \underline{\theta}_a + e_y \qquad (54.b)$$

Expressed by its components $\underline{\phi}$ given as follows

$$\underline{\phi}_a = \begin{vmatrix} \phi_x \\ \phi_y \\ \phi_z \end{vmatrix} \qquad (55)$$

however, the angles which constitute the components of are defined in the FHST coordinate system. Therefore, to keep using the same angles we write $\underline{\phi}_a = M_T^{T,ass}\, \underline{\phi}$. But $M_T^{T,ass} = I - [\underline{\phi}x]$, therefore $M_T^{T,ass}\, \underline{\phi} = \underline{\phi} - [\underline{\phi}x]\underline{\phi} = \underline{\phi}$. Consequently,

$$\underline{\phi}_a = \underline{\phi} \qquad (56)$$

When (56) is substituted into (54) we obtain

$$z_1 = (\underline{m}_1 \times \underline{S}_c) \cdot \underline{\phi} + (\underline{m}_1 \times \underline{S}_c) \cdot \underline{\theta}_a + e_x \qquad (57.a)$$

$$z_2 = (\underline{m}_2 \times \underline{S}_c) \cdot \underline{\phi} + (\underline{m}_2 \times \underline{S}_c) \cdot \underline{\theta}_a + e_y \qquad (57.b)$$

We can write (57) as follows

$$\begin{bmatrix} z_1 \\ z_2 \end{bmatrix} = \begin{bmatrix} (\underline{m}_1 \times \underline{S}_c)' \\ (\underline{m}_2 \times \underline{S}_c)' \end{bmatrix} \begin{bmatrix} \varphi \\ \vartheta \\ \psi \end{bmatrix} + \begin{bmatrix} (\underline{m}_1 \times \underline{S}_c)' \\ (\underline{m}_2 \times \underline{S}_c)' \end{bmatrix} \begin{bmatrix} \phi_x \\ \phi_x \\ \phi_z \end{bmatrix} + \begin{bmatrix} e_x \\ e_y \\ 0 \end{bmatrix} \quad \ldots (58.a)$$

where ' denotes the transpose. This equation is the measurement model of a generic FHST. Each one of the two FHST has such a measurement equation. Writing (58) in terms of the state vector $\underline{X}$ and thus forming the measurement matrix, H, is straight forward. The matrix which corresponds to this measurement equation for the first FHSS is

$${}^1H_F = \begin{bmatrix} (\underline{m}_1 \times \underline{S}_c)' \\ (\underline{m}_2 \times \underline{S}_c)' \end{bmatrix} \quad 0_{2X12} \quad \begin{bmatrix} (\underline{m}_1 \times \underline{S}_c)' \\ (\underline{m}_2 \times \underline{S}_c)' \end{bmatrix} \quad 0_{2x6} \quad \ldots (58.b)$$

and the matrix for the second FHST is

$${}^2H_F = \begin{bmatrix} (\underline{m}_1 \times \underline{S}_c)' \\ (\underline{m}_2 \times \underline{S}_c)' \end{bmatrix} \quad 0_{2X15} \quad \begin{bmatrix} (\underline{m}_1 \times \underline{S}_c)' \\ (\underline{m}_2 \times \underline{S}_c)' \end{bmatrix} \quad 0_{2x3} \quad \ldots (58.c)$$

FSS measurement model

The geometry of the FSS measurement is similar to that of the FHST presented in Fig. 4. Here, however, we cannot assume that the angles A and B are small; that is, the Sun vector is not nearly coincidental with the boresight line. Therefore all the developments that were based on this assumption are not valid in the development of the FSS error model. Consequently a different approach has to be taken. It is evident that $\underline{S}$ shown in Fig.4, can be expressed in the FSS coordinates, s, as follows

$$\underline{S}_s' = [-\tan A, \ -\tan B, \ 1]d \quad (59.a)$$

$$d = [(\tan A)^2 + (\tan B)^2 + 1]^{-1/2} \quad (59.b)$$

Let $\underline{S}_{s,ass}$ denote a column matrix whose elements are the components of $\underline{S}$ in the *assumed* (non-misaligned) FSS coordinates. The relationship between this vector and $\underline{S}_s$ is given by

$$\underline{S}_s = G_s^{s,ass} \underline{S}_{s,ass} \quad (60)$$

where $G_s^{s,ass}$ is the transformation matrix from the assumed to the fine Sun sensor coordinates. In analogy to (42) we can write

$$G_s^{s,ass} = I - [{}^s\underline{\phi} x] \quad (61)$$

where

$$-[{}^s\underline{\phi} x] = \begin{bmatrix} 0 & {}^s\phi_z & -{}^s\phi_y \\ -{}^s\phi_z & 0 & {}^s\phi_x \\ {}^s\phi_y & -{}^s\phi_x & 0 \end{bmatrix} \quad (62)$$

Substitution of (61) into (60) yields

$$\underline{S}_s = \underline{S}_{s,ass} - [{}^s\underline{\phi} x] \underline{S}_{s,ass} \quad (63)$$

From (63) we immediately realize that if instead of $\underline{S}_{s,ass}$ we use $\underline{S}_s$, we introduce an error due to the FSS misalignment. This error is $-[{}^s\underline{\phi} x] \underline{S}_{s,ass}$.

The FSS outputs are really $(\tan A)_m$ and $(\tan B)_m$ where (see fig.4) $\tan A = S_x/h$ and $\tan B = S_y/h$. The subscript m denotes the measured tanA and tanB. Define the following column matrix

$$\underline{S}_{s,m}' = [-(\tan A)_m, \ -(\tan B)_m, \ 1]d_m \quad (64.a)$$

$$d_m = [(\tan A)_m^2 + (\tan B)_m^2 + 1]^{-1/2} \quad (64.b)$$

Let $u_m = (\tan A)_m$ and $v_m = (\tan B)_m$, then (64) can be written as

$$\underline{S}_{s,m}' = [-u_m, \ -v_m, \ 1]d_m \quad (65.a)$$

$$d_m = [u_m^2 + v_m^2 + 1]^{-1/2} \quad (65.b)$$

Furthermore, using Taylor series expansion we can write [9]

where $$\underline{S}_{s,m}' = \underline{S}_s + d\underline{S} \quad (66)$$

$$d\underline{S} = \begin{bmatrix} W_{11} & W_{12} \\ W_{21} & W_{22} \\ W_{31} & W_{23} \end{bmatrix} \begin{bmatrix} e_x \\ e_y \end{bmatrix} = W\underline{e} \quad (67)$$

The matrix W is evaluated as follows [9]

$$\begin{aligned} W_{11} &= d_m - d_m^3 u_m^2 & W_{12} &= -d_m^3 u_m v_m \\ W_{21} &= W_{12} & W_{22} &= d_m - d_m^3 v_m^2 \\ W_{31} &= -d_m^3 & W_{32} &= -d_m^3 v_m \end{aligned} \quad (68)$$

and e_x and e_y are the additive measurement errors involved in measuring tanA and tanB respectively. From (66) and (67) we obtain

$$\underline{S}_{s,m} = \underline{S}_s + W\underline{e} \quad (69)$$

Substitution of (63) into (69) yields

$$\underline{S}_{s,m} = \underline{S}_{s,ass} - [{}^s\underline{\phi} x] \underline{S}_{s,ass} + W\underline{e} \quad (70)$$

Next we compute the estimate of $\underline{S}_s$. We denote the computed value by $\underline{S}_{s,c}$. The computation is carried out as follows

$$\underline{S}_{s,c} = G_{s,ass}^a T_c^I \underline{S}_I \quad (71)$$

In (71) we actually have to use the matrix T_a^I; however, since this matrix is unknown to us we use T_c^I instead. $\underline{S}_I$ is taken from the ephemeris. From (33)-(35)

$$T_c^I = (I - [\underline{\theta} x]) T_a^I$$

Thus (71) can be written as

$$\underline{S}_{s,c} = G_{s,ass}^a (I - [\underline{\theta} x]) T_a^I \underline{S}_I$$

which can be written as

$$\underline{S}_{s,c} = G_{s,ass}^a \underline{S}_a - G_{s,ass}^a [\underline{\theta} x] \underline{S}_a$$

where $\underline{S}_a$ is a column matrix whose elements are the components of $\underline{S}$ when the latter is resolved in the

body, a, coordinate system. Note that since $G^a_{s,ass}$ is orthogonal

$$- G^a_{s,ass}[\underline{\theta}\times]\underline{S}_a = - (G^s_{s,ass}\underline{\theta}) \times G^a_{s,ass}\underline{S}_a = - (G^a_{s,ass}\underline{\theta}) \times \underline{S}_{s,as}$$

Using the last equation, we can write the former as

$$\underline{S}_{s,c} = \underline{S}_{a,ass} - (G^a_{s,ass}\underline{\theta}) \times \underline{S}_{s,ass} \qquad (72)$$

Now define the first component of the effective measurement (which is to be processed by the EKF) as follows

$$z_1 = (\underline{S}_{s,m} - \underline{S}_{s,c})_x \qquad (73)$$

where $(\ )_x$ denotes the x component of the expression in the brackets. When (70) and (72) are substituted into (73), we obtain

$$z_1 = (\underline{S}_{s,ass} - [{}^s\underline{\phi}\times]\,\underline{S}_{s,ass} + \underline{We} - \underline{S}_{a,ass} + (G^a_{s,ass}\underline{\theta}) \times \underline{S}_{s,ass})_x$$

which yields

$$z_1 = (- [\underline{S}_{s,ass}\times]G^a_{s,ass}\underline{\theta} + \underline{S}_{s,ass} \times {}^s\underline{\phi} + \underline{We})_x \qquad (74)$$

Following the rationale that led to (56), we can substitute $\underline{S}_{s,ass}$ in (74) by $\underline{S}_{s,m}$ with practically no loss of accuracy. In addition, we use the notation

$$G^a_{s,ass} = [\underline{q}_1,\ \underline{q}_2,\ \underline{q}_3] \qquad (75)$$

therefore (74) can be written as

$$z_1 = ([-\underline{S}_{s,m}\times][\underline{q}_1,\ \underline{q}_2,\ \underline{q}_3]\underline{\theta} + \underline{S}_{s,m} \times {}^s\underline{\phi} + \underline{We})_x \qquad (76.a)$$

To compute z_2 we apply the foregoing development but now we use the y rather than the x component. This will yield a result similar to (76.a); namely,

$$z_2 = ([-\underline{S}_{s,m}\times][\underline{q}_1,\ \underline{q}_2,\ \underline{q}_3]\underline{\theta} + \underline{S}_{s,m} \times {}^s\underline{\phi} + \underline{We})_y \qquad (76.b)$$

The last two equations can be put in the following form

$$\begin{bmatrix} z_1 \\ z_2 \end{bmatrix} = \left|\underline{q}_1\times\underline{S}_{s,m},\ \underline{q}_2\times\underline{S}_{s,m},\ \underline{q}_3\times\underline{S}_{s,m}\right|_2 \begin{bmatrix} \varphi \\ \vartheta \\ \psi \end{bmatrix} + \left|[\underline{S}_{s,m}\times]\right|_2 \begin{bmatrix} {}^s\phi_x \\ {}^s\phi_y \\ {}^s\phi_z \end{bmatrix} + W_2 \begin{bmatrix} e_x \\ e_y \\ 0 \end{bmatrix} \qquad \ldots (77.a)$$

where the subscript 2 denotes the first two rows of a matrix. The measurement matrix, H_s which corresponds to this measurement equation is given by

$$H_s = \left|\underline{q}_1\times\underline{S}_{s,m},\ \underline{q}_2\times\underline{S}_{s,m},\ \underline{q}_3\times\underline{S}_{s,m}\right| \quad 0_{3x24} \quad \left|[\underline{S}_{s,m}\times]\right|_2 \qquad \ldots (77.b)$$

Note that the 3rd row of the square matrices in (77) is omitted. This completes the development of the "truth model". To sum it up, the dynamics model is given by (30), the FHST measurement model is given by (58) and it fits either one of the two FHSTs, and finally, the measurement model of the FSS is given by (77).

2.3. THE DESIGN MODEL

Error Propagation Model

The "design model" is the simplified, reduced order model which is assumed to be the model of the system for the OBC filter design purposes. The following assumptions are made in the design of the EUVE Update Filter. The gyro scale factor errors and misalignments are negligible (or fully compensated for). The FHSTs and the FSS are perfectly aligned. With these assumptions the error propagation equation of the "truth model" reduces to

$$\begin{bmatrix} \dot{\varphi} \\ \dot{\vartheta} \\ \dot{\psi} \\ \dot{u}_x \\ \dot{u}_y \\ \dot{u}_z \end{bmatrix} = \begin{bmatrix} 0 & w_z & -w_y & -1 & 0 & 0 \\ -w_z & 0 & w_x & 0 & -1 & 0 \\ w_y & -w_x & 0 & 0 & 0 & -1 \\ 0 & 0 & 0 & 0 & 0 & 0 \\ 0 & 0 & 0 & 0 & 0 & 0 \\ 0 & 0 & 0 & 0 & 0 & 0 \end{bmatrix} \begin{bmatrix} \varphi \\ \vartheta \\ \psi \\ u_x \\ u_y \\ u_z \end{bmatrix} + \begin{bmatrix} w_{1x} \\ w_{1y} \\ w_{1z} \\ w_{2x} \\ w_{2y} \\ w_{2z} \end{bmatrix} \qquad \ldots (78)$$

This model can be expressed as

$$\underline{\dot{X}}^* = A^*\underline{X}^* + \underline{n}^* \qquad (79)$$

where $\underline{X}^*$, A^* and $\underline{n}^*$ are defined in (25).

Measurement Model

Star tracker measurements

With the assumption mentioned before and corresponding to the "design model" of (78), The FHST measurement matrix of either star tracker reduces to

$$\begin{bmatrix} z_1 \\ z_2 \end{bmatrix} = \begin{bmatrix} (\underline{m}_1 \times \underline{S}_c)' \\ (\underline{m}_2 \times \underline{S}_c)' \end{bmatrix} \begin{bmatrix} \varphi \\ \vartheta \\ \psi \end{bmatrix} + \begin{bmatrix} e_x \\ e_y \\ 0 \end{bmatrix} \qquad (80.a)$$

This yields the following measurement matrix

$$H^*_F = \begin{bmatrix} (\underline{m}_1 \times \underline{S}_c)' \\ \underline{m}_2 \times \underline{S}_c)' \end{bmatrix} \quad 0_{2x3} \qquad (80.b)$$

It is easily seen that this is the measurement matrix for either FHST.

Sun sensor measurements

Corresponding to the state vector of the "design model" the FSS measurement equation is reduced to

$$\begin{bmatrix} z_1 \\ z_2 \end{bmatrix} = \begin{bmatrix} g_1 \times \underline{S}_{s,m},\ g_2 \times \underline{S}_{s,m},\ g_3 \times \underline{S}_{s,m} \end{bmatrix}_2 \begin{bmatrix} \varphi \\ \vartheta \\ \psi \end{bmatrix} + W_2 \begin{bmatrix} e_x \\ e_y \end{bmatrix} \quad \ldots (81.a)$$

The corresponding measurement matrix is

$$H_s^* = \begin{bmatrix} g_1 \times \underline{S}_{s,m},\ g_2 \times \underline{S}_{s,m},\ g_3 \times \underline{S}_{s,m} \end{bmatrix} \begin{bmatrix} 0_{3x3} \end{bmatrix}_2 \quad (81.b)$$

3.0 TRUE COVARIANCE SIMULATION ALGORITHM

To present the so-called "true covariance" simulation algorithm whose development is introduced in [6], we have to define, D, the transformation matrix from the state vector of the "truth model" to that of the "design model". It is easy to see that in our case

$$D = [I_{6x6} \mid 0_{6x18}] \quad (82)$$

Using D we define the following matrices

$$dA = DA - A^*D \quad (83.a)$$

where A is the 24x24 matrix defined in (30). The matrixes A, A^* and dA are then used to define A^C as follows

$$A^C = \begin{bmatrix} A & 0 \\ dA & A^* \end{bmatrix} \quad (83.b)$$

Next, we discretize the matrices A^C and Q^* where the latter is the spectral density matrix of the white noise vector driving the dynamics part of the "design model" given in (78). The discretization algorithm is given in [5, pp. 296 - 299]. The discretization is denoted as follows

$$A^C \dashrightarrow \Phi^C_{k-1}$$

$$Q^* \dashrightarrow Q^*_{k-1}$$

With Q^*_{k-1} on hand, we compute Q^C_{k-1} as follows

$$Q^C_{k-1} = \begin{bmatrix} I \\ D \end{bmatrix} Q^* \begin{bmatrix} I & D^T \end{bmatrix} \quad (84)$$

In our case, all the preceding matrices are constant and need to be computed only once.

Between measurement updates we propagate the matrices C_k and P^*_k as follows

$$C_k(-) = \Phi^C_{k-1}\, C_{k-1}\, \Phi^C_{k-1}{}' + Q^C_{k-1} \quad (85.a)$$

$$P^*_k(-) = \Phi^*_{k-1}\, P^*_{k-1}(+)\, \Phi^*_{k-1}{}' + Q^*_{k-1} \quad (85.b)$$

where C_k is the second moment matrix of the augmented state vector whose entries are, from top to bottom, the state vector of the "truth model" given in (30), and a vector which is the difference between the state esimate generated by the OBC EKF and the correct value of this state. Note that the second vector, which has 6 components, is the correct estimation error vector. Therefore the last 6 elements on the main diagonal of C_k are the mean squre errors of the filter estimation error and their evaluation is the goal of the "true covariance" analysis. In contrast to these 6 elements, the 6 elements on the main diagonal of P^*_k are the apparent variances of the estimation error states. That is, if the "truth model" were identical to the "design model", these elements would have been the variances of the estimation error.

When a measurement is acquired, the following computations are carried out

$$K^*_k = P^*_k(-)H^*_k{}' \, [H^*_k P^*_k(-) H^*_k{}' + R^*_k]^{-1} \quad (86.a)$$

$$P^*_k(+) = [I - K^*_k H^*_k]\, P^*_k(-)\, [I - K^*_k H^*_k]' + K^*_k R^*_k K^*_k{}' \quad (86.b)$$

$$dH_k = H_k - H^*_k D \quad (86.c)$$

$$B_k = \begin{bmatrix} I & 0 \\ -K^*_k dH_k & I - K^*_k H^*_k \end{bmatrix} \quad (86.d)$$

$$C_k(+) = B_k\, C_k(-)\, B_k{}' + K^C_k\, R_k\, K^C_k{}' \quad (86.e)$$

4.0 CASE STUDY OBJECTIVES AND RESULTS

There were three primary objectives in the case studies. First, the performance of the EP filter was examined in the ideal situation when its model was equivalent to the truth model. Secondly, the expected onorbit behavior of the filter was examined. Lastly, a sensitivity analysis was performed. The cases studied were as follows:

- Case 1: No Errors
- Case 2: Expected Errors
- Case 3: Sensitivity Analysis
  - 3A: Gyro white noise about each axis
  - 3B: Gyro random walk about each axis
  - 3C: Gyro Misalignments about each axis
  - 3D: Gyro Scale factor errors about each axis
  - 3E: FHST noise
  - 3F: FHST # 2 misalignments about each axis
  - 3G: FSS noise
  - 3H: FSS misalignments about each axis

Each simulation was ten minutes. The attitude and gyro drift estimation errors were determined by the truth model and update filter. The results in sections 4.1, 4.2, and 4.3 represent the truth model determined estimation errors. The following is a listing of nominal simulation input values:

Initial State Variances

Initial Attitude Error: 1800 arcsec/axis
Initial Drift Rate Bias: 0.5 arcsec/sec/axis

Dynamic Noise Inputs

IRU White Noise drift (roll): $(0.68936 \text{ arcsec/sec}^{1/2})^2$
(pitch and yaw axes): $(4.246E\text{-}2 \text{ arcsec/sec}^{1/2})^2$
IRU Random Walk Drift: $(4.4413E\text{-}5 \text{ arcsec/sec}^{3/2})^2$/axis

Measurement Noise Input

FHST Measurment Noise Variances: $(14 \text{ arcsec})^2$
FSS Measurement Noise Variances: $(24.4131 \text{ arcsec})^2$

4.1 Case 1: No errors

The following case demonstates the performance of the filter in the ideal case when the truth model was identical to the design model. The final attitude and gyro drift errors were as follows:

Attitude Estimation Errors
(arcseconds)

Roll	Pitch	Yaw
4.8784	2.8321	2.5080

Gyro Drift Estimation Errors
(arcseconds/second)

Roll	Pitch	Yaw
3.022E-2	0.9103E-2	8.313E-3

4.2 Case 2: Expected Errors

This case demonstrates the expected performance of the filter on orbit. The attitude is defined relative to one of the FHSTs (#1 in our simulations). Thus, the obtained attitude accuracy is on the order of the accuracy of the FHSTs which are the primary attitude sensor. The following are additional expected on orbit input errors:

FHST #1 Misalignment: 0 arcseconds/axis
FHST #2 Misalignment: 24 arcseconds/axis
FSS Misalignment: 36 arcseconds/axis
Gyro Scale Factor Error: 1000 ppm/axis
Gyro Misalignment: 8 arcseconds/axis

The results are the following:

Attitude Estimation Errors
(arcseconds)

Roll	Pitch	Yaw
16.5005	19.1984	13.0119

Gyro Drift Estimation Errors
(arcseconds/second)

Roll	Pitch	Yaw
3.2513E-2	5.1160E-2	6.9354E-2

Comparing these values to the ideal case, one can see errors induced by only considering a subset of the true state vector in state estimation. The attitude estimation errors are off by several orders of magnitude and the gyro drift estimation errors are off almost an order of magnitude.

4.3 Case 3: Sensitivity Analysis

In the following simulations, the sensitivity of onboard filter to additional attitude sensor noises, misalignments, and scale factor errors was tested. These errors were applied separately to each sensor axis, and the resulting attitude and gyro drift estimation errors were observed. Sensitivity to the various error sources were determined in the following manner about each spacecraft axis (where applicable):

Dynamic noise (white & random walk): 3x nominal/axis
FHST #2 Misalignments: 2x nominal/axis
FSS Misalignments: 2x nominal/axis
Measurement noise (FHSTs & FSS): 2x nominal

The following tables and figures demonstrate the filter performance due to the increased errors.

Attitude Estimation Errors (arcseconds)

Case	Axis	Roll	Pitch	Yaw
3A	x	18.6886	19.1984	13.0119
3A	y	16.5006	19.2332	13.0179
3A	z	16.5005	19.2065	13.0435
3B	x	16.5007	19.1984	13.0119
3B	y	16.5005	19.1994	13.0121
3B	z	16.5005	19.1987	13.0125
3C	x	16.5005	19.1984	13.0119
3C	y	16.5005	19.1984	13.0119
3C	z	16.5005	19.1984	13.0119
3D	x	16.5005	19.1984	13.0119
3D	y	16.5005	19.1984	13.0119
3D	z	16.5005	19.1984	13.0119
3E		19.1600	25.7578	18.0298
3F	x	27.2160	29.6328	15.9332
3F	y	22.3209	25.5485	13.0534
3F	z	17.3819	19.3448	21.7191
3G		16.9075	18.9557	13.0284
3H	x	16.7568	24.9939	13.1199
3H	y	16.8615	19.8543	16.3459
3H	z	16.5005	19.1984	13.0119

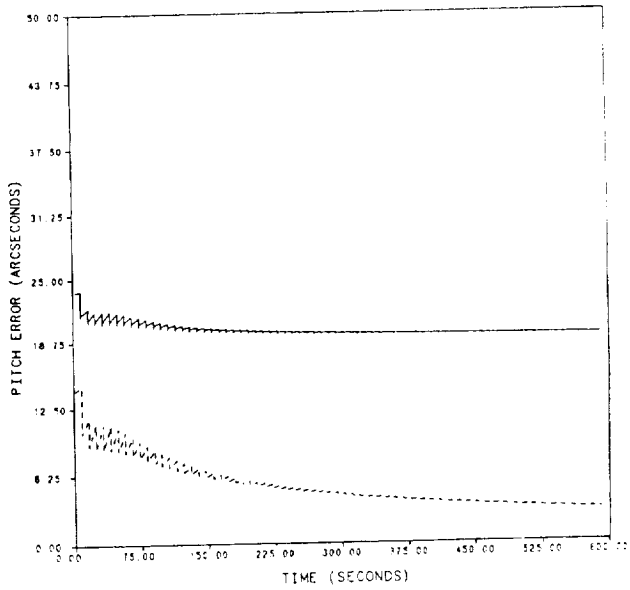

Fig. 5: The standard deviation of the pitch estimation error vs. time. (The solid line is that of the true error, and the dashed line is of the error predicted by the update filter covariance matrix.)

The time history of the standard deviations of the attitude and gyro drift estimation errors was plotted for Case 2 (expected onorbit errors). The results about each axis were found to be similar. A typical plot (pitch attitude error) is presented in Fig. 5.

Gyro Drift Estimation Errors
(arcseconds/second)

Case	Axis	Roll	Pitch	Yaw
3A	x	8.7164E-2	5.1160E-2	6.9354E-2
3A	y	3.2513E-2	5.1451E-2	6.9364E-2
3A	z	3.2513E-2	5.1202E-2	6.9566E-2
3B	x	3.2564E-2	5.1160E-2	6.9354E-2
3B	y	3.2513E-2	5.1197E-2	6.9355E-2
3B	z	3.2513E-2	5.1161E-2	6.9378E-2

3C	x	3.2513E-2	5.1160E-2	6.9354E-2
3C	y	3.2513E-2	6.8993E-2	6.9354E-2
3C	z	3.2513E-2	5.1160E-2	8.3385E-2
3D	x	3.8577E-2	5.1160E-2	6.9354E-2
3D	y	3.2513E-2	5.1160E-2	6.9354E-2
3D	z	3.2513E-2	5.1160E-2	6.9354E-2
3E		3.5639E-2	6.5980E-2	8.9894E-2
3F	x	3.2513E-2	5.9675E-2	10.2473E-2
3F	y	3.2513E-2	5.1277E-2	8.9347E-2
3F	z	3.2513E-2	7.7423E-2	6.9809E-2

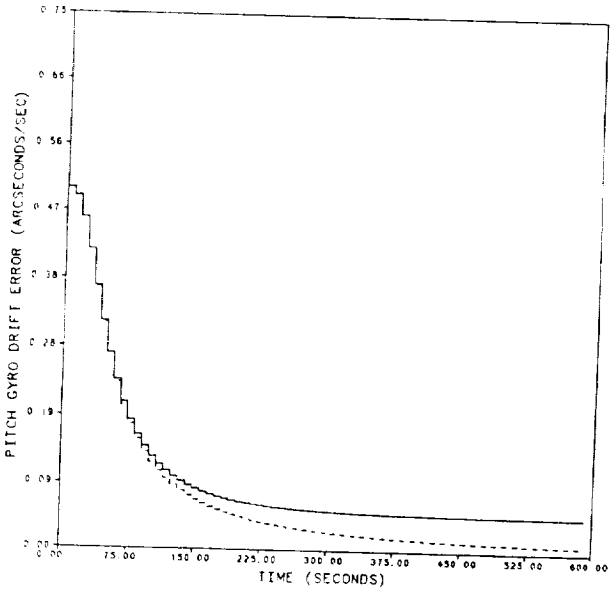

Fig. 6: The standard deviation of the pitch gyro drift estimation error vs. time. (The solid line is that of the true error, and the dashed is of the error predicted by the update filter covariance matrix.)

3G		3.2543E-2	5.1259E-2	6.8545E-2
3H	x	3.2513E-2	5.1467E-2	8.7576E-2
3H	y	3.2513E-2	6.0912E-2	7.1389E-2
3H	z	3.2513E-2	5.1160E-2	6.9354E-2

A typical plot for gyro drift error is presented in Fig. 6.

Of the gyro noises, the white noise component had the most effect on the filter performance. As expected, the effect was confined primarily to the axis being corrupted. When the X-axis gyro white noise was increased by 3x, the roll gyro drift estimation error jumped 5.0E-2 arcseconds/second, and the roll estimation errors jumped approximately 2 arcseconds. The effect of an increase in pitch and yaw gyro white noise had a very nominal affect on estimation errors. Since EUVE has a roll rate of 3 RPO, the roll gyro has to use less accurate gyro data as compared to the pitch and yaw axes which are approximately inertial. This inaccuracy in roll gyro data is modeled by an increase in the white noise component in the roll gyro data. Thus, an increase in the white noise about the roll axis affects the attitude much more significantly than an increase about the pitch and yaw axes. The gyro misalignments about the pitch and yaw axes corrupted their respective drift estimates significantly due to their projections picking up the relatively high roll rate. The roll axis misalignments have no effect due to zero yaw and pitch rates. The gyro scale factors only showed up in the roll gyro drift estimation error due the above mentioned high relavive roll rate and 0 pitch and yaw rates. The FHST #2 misalignments were the largest contributer to attitude and gyro drift estimation errors as expected with the FHST X-axis misalignment causing roll and pitch errors of 27.2 and 29.6 arcseconds. The FHST Z-axis caused a yaw error of 21.7 arcseconds. The FSS misalignments affect on the attitude and gyro drift estimation errors were significant but not as significant as the FHSTs due to the larger sensor noise variance. The FSS X-axis misalignment translated into a pitch error of 24.9 arcseconds while a Y-axis misalignment caused roll and yaw attitude errors of 16.8 and 16.3 arcseconds respectively. The FHST measurement noise increases affected the attitude estimation errors almost as much as the FHST misalignments with roll, pitch, and yaw errors of 19.1, 25.7, and 18.0 arcseconds respectively. An increase in FSS measurement noise had a relatively small effect on estimation errors. The resulting roll, pitch, and yaw attitude errors were 16.9, 18.9, and 13.0 arcseconds respectively. The pitch attitude estimation error went down slightly as compared to the nominal simulation, and the roll and yaw attitude errors increased slightly. The reason the attitude estimation errors were affected so little as compared to the increased FHST noise simulation was due to the filter weighting the more accurate FHST measurements heavier than the less accurate FSS measurements.

5.0 CONCLUSIONS

Of all the errors, the FHST misalignments proved to cause the most significant attitude and gyro drift estimation errors. The roll and pitch estimation errors increased by approximately 10 arcseconds from the nominal estimation errors when the X-axis misalignment of FHST #2 was doubled to 48 arcseconds. Doubling the Z-axis misalignment of FHST #2 increased the yaw estimation errors by approximately 8 arcseconds. The pitch and yaw gyro drift estimation errors were affected most by Z and Y - axis misalignments of FHST #2. An increase in the white noise about the gyro X-axis was responsible for the largest roll gyro drift estimation error. The gyro drift estimation errors only affects the system when measurement update periods are large. EUVE should have a sufficient number of star measurement updates from the FHSTs. If not, the attitude estimation accuracy could degrade significantly. Overall, the results showed the EUVE update filter to be quite robust even though some significant errors were put into the system. This study demonstrated the six states modeled in the filter are the most significant states needed for onboard attitude estimation.

Appendix

Express the two quaternions q_1 and q_2 as follows

$$q_1 = \begin{bmatrix} \\ \underline{r}_1 \\ \cdots \\ p_1 \\ \\ \end{bmatrix} \quad \text{and} \quad q_2 = \begin{bmatrix} \\ \underline{r}_2 \\ \cdots \\ p_2 \\ \\ \end{bmatrix}$$

where $\underline{r}_1$, $\underline{r}_2$ are the vector parts of the respective quaternions and p_1, p_2 are their scalar parts. Then

$$q_1 q_2 = \begin{bmatrix} \underline{r}_1 \times \underline{r}_2 + p_1 \underline{r}_2 + p_2 \underline{r}_1 \\ \cdots\cdots\cdots\cdots\cdots\cdots \\ p_1 p_2 - \underline{r}_1^T \underline{r}_2 \end{bmatrix}$$

The upper part of the column yields three components which are the components of the imaginary part of the quaternion product and the lower part yields the scalar part of the product.

References

1. K. Ha, "EP Update Filter Analysis", Fairchild Space Company, Inter-Office Communication, ACS:EP:035, August 17,1987.

2. K. Ha, "EP Update Filter Development", Fairchild Space Company, Inter-Office Communication, ACS:EP: 88:014, February 9, 1988.

3. M. Frieder, "Gyro Model for Kalman Filter Simulation", Fairchild Space Company, Inter - Office Communication, ACS:EP:87:019, June 11, 1987.

4. M. Frieder, "Star Tracker Model for Kalman Filter Simulation", Fairchild Space Company, Inter - Office Communication, ACS:EP:028, July 17, 1978.

5. A. Gelb, Applied Optimal Estimation, MIT Press, Cambridge MA, 1974.

6. I. Y. Bar-Itzhack, Seminar notes on True Covariance Analysis, Code 554, NASA-GSFC, Oct. 12, 88, p.29.

7. J. C. Wilcox, "A New Algorithm for Strapped-Down Inertial Navigation", IEEE Trans. on Aerosp. and Elect. Syst., Vol. AES-5, Sept. 67, pp.796-802.

8. J. R. Wertz (ed.) Spacecraft Attitude Determination and Control, D. Reidel Publishing Company, Boston, MA, 1978, p. 414.

9. J. Deutschmann and I.Y. Bar-Itzhack, "Extended Kalman Filter for Attitude Estimation of the Earth Radiation Budget Satellite," Flight Mechanics/Estimation Theory Symposium, NASA Goddard Space Flight Center, 23-24 May, 1989.